heritage

Article

# Curved Linear Diode Array Imaging of a Historic Anchor Recovered from East Anglia ONE Offshore Wind Farm

**Brandon Mason [1,*], James Finch [2], Sarah Paynter [3], Heather Anderson [1] and Lauren Nagler [1]**

1 Maritime Archaeology Trust, Southampton SO14 3ZH, UK; heather.anderson@maritimearchaeology.co.uk (H.A.); lauren.nagler@maritimearchaeology.co.uk (L.N.)
2 Nikon Metrology UK, Tring HP23 4JX, UK; james.finch@nikon.com
3 Historic England, Portsmouth PO4 9LD, UK; sarah.paynter@historicengland.org.uk
* Correspondence: brandon.mason@maritimearchaeology.co.uk

**Abstract:** The Industrial Metrology Business Unit of Nikon Corporation, on behalf of ScottishPower Renewables and Maritime Archaeology (MA), Southampton, UK, has employed X-ray CT (computed tomography) to visualise the internal structure of an anchor found in the North Sea. The non-destructive method of internal inspection and measurement has helped to determine approximately when it was made. The results indicate that the artefact, initially thought to be potentially Roman, is probably more recent, likely dating to between the late 16th and early 17th centuries CE. This paper presents the discovery, recovery, analysis and interpretation of a significant find from a UK offshore wind farm and underscores the valuable role that non-destructive X-ray CT played in the investigation.

**Keywords:** anchor; artefact; forging; inspection; iron; measurement; museum; non-destructive; stabilization; X-ray CT; diode array

check for updates

**Citation:** Mason, B.; Finch, J.; Paynter, S.; Anderson, H.; Nagler, L. Curved Linear Diode Array Imaging of a Historic Anchor Recovered from East Anglia ONE Offshore Wind Farm. *Heritage* **2024**, *7*, 2552–2568. https://doi.org/10.3390/heritage7050122

Academic Editors: Silvano Mignardi, Wenke Zhao, Laura Medeghini, Melania Di Fazio and Laura Calzolari

Received: 20 March 2024
Revised: 9 May 2024
Accepted: 10 May 2024
Published: 16 May 2024



## 1. Introduction

Anchor WTG_D_154 was discovered 60 km offshore at a depth of 40 m during remotely operated underwater vehicle (ROV) investigations prior to the development of ScottishPower Renewables' East Anglia ONE offshore wind farm off the coast of Suffolk, UK, in 2018 (Figure 1). The iron anchor, an isolated find, had typological similarities to a late Iron Age example recovered from Bulbury Camp, Dorset, in the 19th century [1,2] as well as other features similar to Roman examples from the 1st–2nd century AD [3,4].

Due to the possible archaeological importance of the anchor, a conservation management plan and long-term care strategy was agreed with Historic England and the anchor was subsequently recovered by ScottishPower Renewables during an archaeological intervention [5].

Dating iron objects is notoriously difficult. Some information can be gained through taking samples from the object for metallography to look for evidence of welds and how the object was constructed. Chemical analysis of the small inclusions of slag waste left in the metal, from when it was smelted or refined, can also indicate the type of fuel used (charcoal or coke) and so suggest a possible date range [6]. Sometimes there is enough carbon in the iron itself to attempt radiocarbon dating [7]. All these methods require samples to be taken, and as it was agreed prior to recovery that the anchor would eventually go on public display, a non-destructive investigative programme of analysis was developed to try to illuminate the mode of construction and the individual elements that comprise the internal structure.

The way that an anchor is constructed provides a possible indication of when it was made. Anchors are typically made from multiple pieces of iron that have been joined together; however, the size and shape of the individual iron pieces, or units, and how these are assembled, tend to change over time. With more developed iron smelting, refining and forging technology, for example, it becomes possible to obtain larger and more uniform pieces of iron and to join many of these to make larger objects.

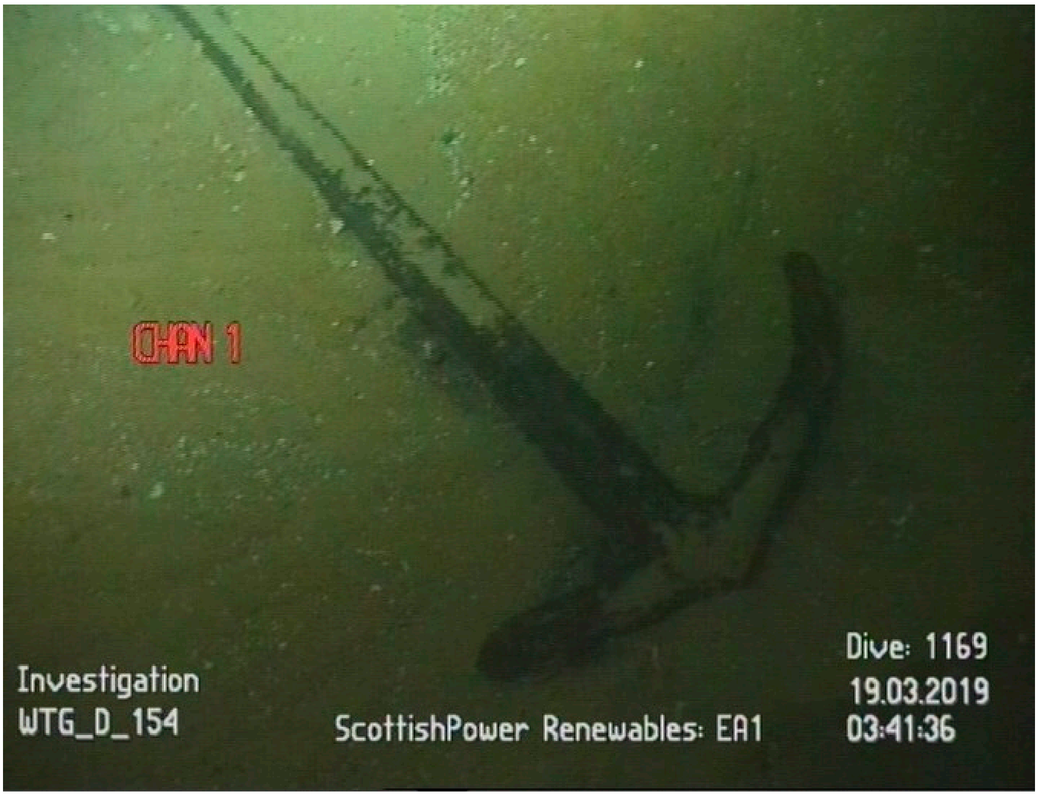


**Figure 1.** Anchor WTG_D_154 on the seabed within East Anglia ONE offshore wind farm developed by ScottishPower Renewables.

Following de-concretion, 2D radiographic imaging was used in an attempt to reveal this internal structure, but with limited results (see Section 2). The anchor was robust, with thick, well-preserved components, and so computed radiography was unable to show any internal features; a more powerful X-ray CT (computed tomography) system was needed to investigate the way the artefact was constructed and to assist in dating it. CT scanning has been used very successfully to investigate objects from shipwrecks, particularly complex composite objects, like pistols or pumps, or to show hidden markings on concreted, fragile metal objects, for example, coins and bells [8,9]. Large CT scanners have been used to investigate ship timbers, which have a comparatively low density, but the application here, with a large metal object, was especially challenging. Following the recommendation of specialists (Dr Peter Northover, School of Archaeology, and Dr Vanessa Cheel, Department of Materials, University of Oxford), Nikon Metrology UK was approached to perform CT scanning of the anchor.

### 1.1. Background

MA (Maritime Archaeology Trust) archaeologists joined vessels involved in unexploded ordnance (UXO) investigation and clearance in August 2018 and March to May 2019 to supervise the recovery of 20 individual objects. The methodology required that objects were brought to deck for detailed assessment and, if appropriate, full archaeological recording.

Anchor WTG_D_154 was identified as a potential UXO by RPS (RPS Group are a contractor specialising in UXO survey) in 2018, based on the review of high-resolution magnetic data collected the previous year. UXO investigation by an ROV (remotely operated underwater vehicle) on 3 March 2018 determined the object to be a possible anchor and it was assigned an initial 20 m radius archaeological exclusion zone (AEZ). The anchor was located in close proximity to a planned wind turbine generator (WTG) (Figure 2).

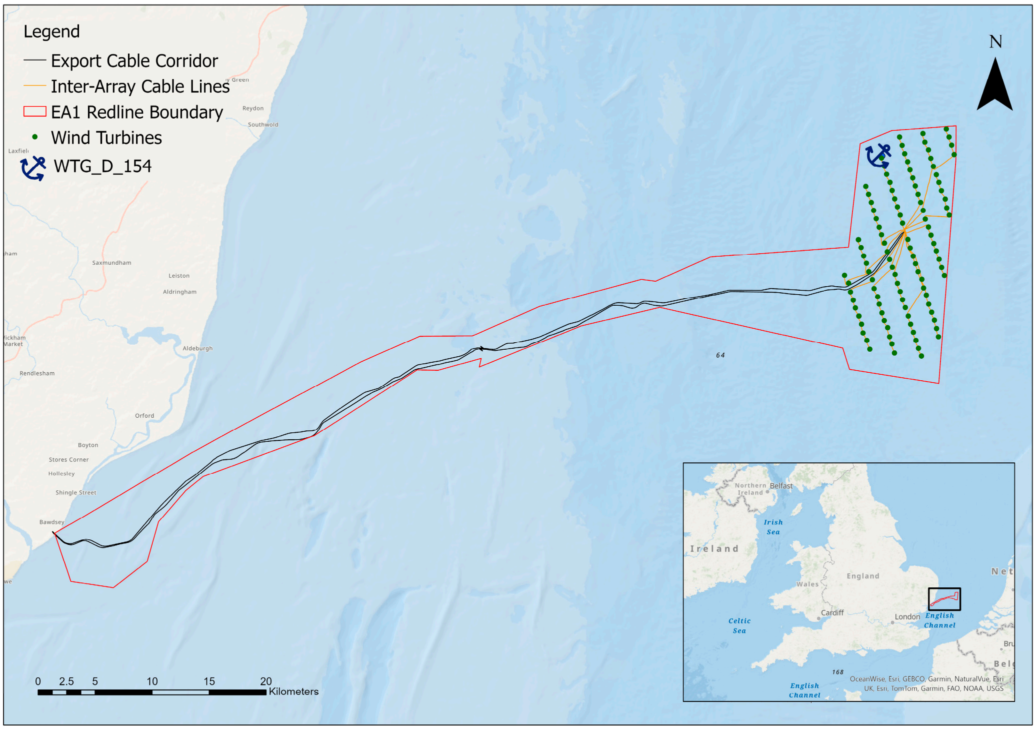


**Figure 2.** Original location of WTG_D_154 within East Anglia ONE offshore wind farm.

The high-resolution magnetic survey demonstrated that there were no related ferrous features within several hundred metres of this find, and it is not directly associated with any complex assemblage.

The location of the feature posed a significant development constraint for the installation of the WTG and so recovery was undertaken between 18–19th March 2019 under archaeological supervision.

The feature was located using a non-ferrous pipe tracker system (Teledyne TSS-440) and was imaged on the seabed using the colour video camera system. It was fully buried with very little concretion apparent. A survey of the anchor before it was lifted showed that the anchor was missing part of one arm, the other apparently in situ but with no evidence of flukes.

Due to the moderate sea conditions and the object size, the anchor was recovered by lifting with a soft strop deployed from the deck crane which was received by the ROV at 5 m altitude. The strop was attached around the anchor throat, generally the strongest and most balanced part of an anchor. This resulted in a simple and effective recovery without further damage to the archaeological material.

This anchor was one of the longest recovered during the investigation campaign and appeared to be relatively unassuming. The head was broken before any type of stock keys or eye, with corrosion products most apparent on the lower surface, i.e., the main point of seabed contact. The crown (to the left in Figure 3) was pointed, with straight arms that swept upwards at the end of the surviving element into a point. One arm was broken with a jagged end before the sweep.

The overall length was 2.23 m, with the crown to arm end length at 0.68 m, giving an overall width of 0.94 m. The shank seemed to be square in section at the throat, sided 0.11 m, though the concretion on the lower side made it difficult to be certain.

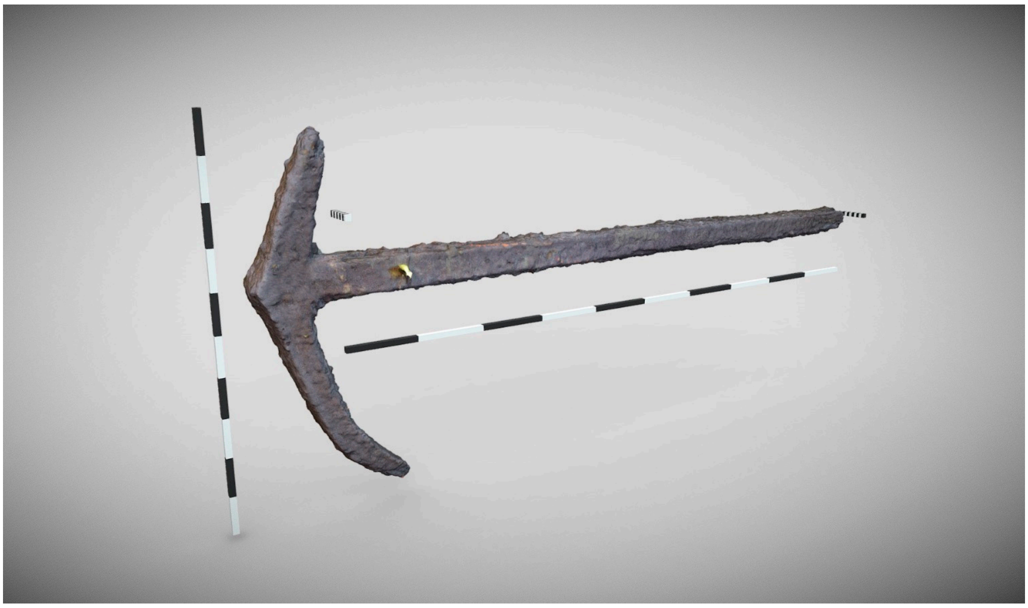

**Figure 3.** Anchor WTG_D_154, represented as a 3D textured mesh following rapid photogrammetry on deck prior to seabed relocation. Scales are 1 m (vertical) and 2 m (horizontal) in length.

At the time of recovery, it was considered that this was a somewhat unusual example of an old-pattern Admiralty longshank anchor, based on the remarkable condition, the overall proportions and the lack of unique features being recognised prior to redeposition.

However, due to some uncertainty about the date or archaeological importance of the anchor, it was selected for photogrammetric recording in the 30 min that it remained on deck from 04:15 to 04:45 a.m. A 3D model of each side was subsequently created (Figure 3—https://skfb.ly/ozG7K) (accessed on 9 May 2024). The object was tagged and returned to the seabed by soft strop and imaged with the ROV in the new location.

In June 2021, Anchor WTG_D_154 was relocated and recovered to the deck of *Glomar Wave* before being brought to shore at Great Yarmouth to commence a programme of conservation and analysis that is still ongoing at the time of writing (Figure 4).

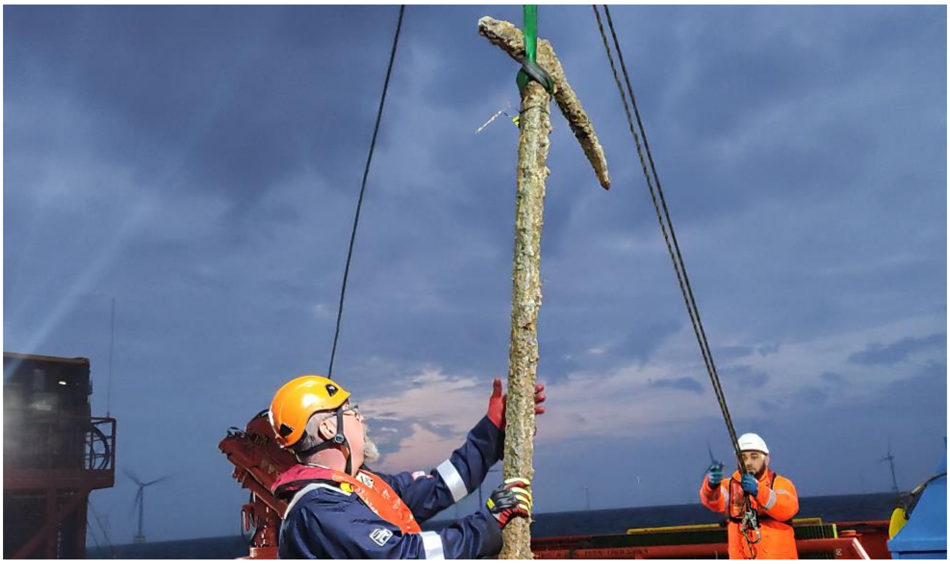

**Figure 4.** Anchor WTG_D_154 arrives safely on the deck of *Glomar Wave* following a recovery operation lasting several hours in June 2021.

### 1.2. Anchor Form and Typology

While robust iron anchors of the 18th to 19th centuries are relatively common, WTG_D_154 is smaller than typical and the arms exhibit a more unusual, segmented form (with a bend approximately halfway along the otherwise straight arms, as opposed to fully straight or curved arms). The recovered anchor was considered to have the potential to be of pre-Viking origin based on the pointed crown, the shape and apparently rectangular cross-section of the shank and arms, and the absence of flukes. These features were unusual for anchors from other periods: for example, Viking, or Scandinavian, anchors typically had straight arms with a triangular cross-section [10] (p. 40), and French 18th-century anchors commonly featured curved arms, while 18th-century English anchors generally had straight arms [11] (p. 93).

While some Renaissance-period Spanish anchors exhibit a similar segmented form of the arms, Spanish anchors were known for being far less robust than this example, particularly around the throat, giving rise to the term "to be as meagre as a Spanish anchor" [11] (p. 52). The present example is extremely robust and is slightly rectangular in cross-section.

Despite this, the typological evidence was suggestive of the type of anchors in use around 2000 years ago, both Roman Imperial and also best represented by the Bulbury anchor, c. 1st century AD [1,2], recovered from the excavations at Bulbury Hillfort in Dorset in the late 19th century and now in the collection at Dorchester Museum (Figure 5). The Bulbury example has been attributed to the Celtic Veneti tribe [1].

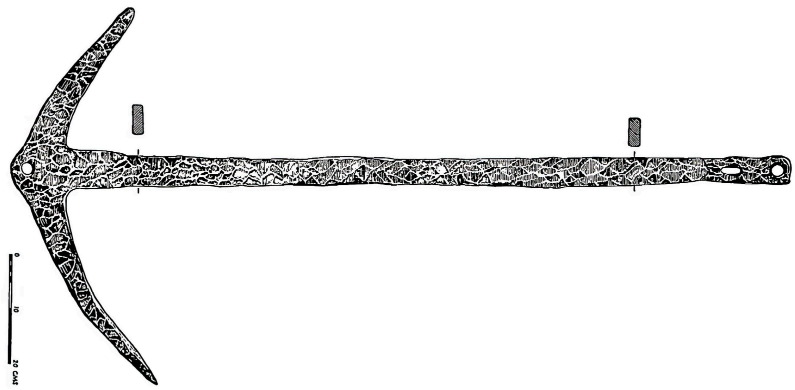

**Figure 5.** Drawing of the iron anchor excavated at Bulbury Camp by Edward Cunnington, 1881 (Reprinted with permission from Dorset Natural History and Archaeological Society, 1884).

The late British maritime archaeologist Keith Muckelroy reflected on how unusual such a find really would be if the pre-Viking date were to be confirmed: "The chances of ever identifying an Iron Age anchor in British or northern French waters would seem to be remote, since one would only have survived over such a period in very exceptional circumstances, and in any case it would be superficially indistinguishable from a modern iron one" [12] (149).

## 2. Materials and Methods

A post-recovery conservation plan was agreed with Historic England [13] and the anchor was given over to the care of Mary Rose Archaeological Services, Portsmouth, for a programme of passive conservation following transfer from Great Yarmouth. The outer layer of encrusting marine sediment and organics fused with corrosion deposits leeched from the anchor, known as marine iron concretion, was carefully removed with chisels and brushes, revealing the corroded wrought iron surface within (Figure 6).

**Figure 6.** Anchor WTG_D_154 partially de-concreted during a conservation programme undertaken by Mary Rose Archaeological Services (Image used with permission from Mary Rose Trust, 2022).

Preliminary radiography at 325 kV undertaken by Historic England at Fort Cumberland, Portsmouth, UK, could not penetrate the well-preserved iron, but the results did show that the structure was of a high density and also ruled out any suggestion of a hole through the crown, a feature often seen on Roman and Scandinavian anchors for securing the anchor to the hull when not deployed [14].

*CT Scanning*

Due to this overall external similarity of iron anchors over two millennia, a deeper understanding of the internal structure was required, and Nikon Metrology UK (https://industry.nikon.com, accessed on 9 May 2024) offered experience and support to obtain imagery that could achieve this aim. CT scanning was carried out pro bono during January 2023 at Nikon's centre in Tring, UK, where machines are available for subcontract inspection, and where all of the X-ray sources for Nikon group's industrial X-ray CT systems are manufactured. At this stage the anchor was part way through desalination treatment so it was constantly wrapped in capillary matting saturated with fresh water while it was out of the treatment tank. The study had to be completed in a single day to avoid damage caused by uncontrolled drying.

The size and shape of the anchor posed some challenges for the works, since the weight of the object meant that a significant support structure was needed to hold the anchor in place during imaging. Additionally, the shape of the anchor meant extra considerations were needed in order to obtain the best resolution scan data while preventing any collisions between the target material and the X-ray system source. It was decided to position the anchor at an angle of approximately 25 degrees from vertical to distribute the weight over the bottom area of the anchor (to prevent accidental damage to the X-ray system or the anchor itself while the scan took place), and to have the arms of the anchor rotate below the X-ray source. This gave the best compromise of support for the anchor and the best chance for acquiring high-resolution data (Figure 7).

**Figure 7.** Positioning the anchor on a wooden frame within the Nikon C2 X-ray CT system.

The works carried out at Nikon utilised the C2, large-envelope, X-ray CT system with a Nikon 450 kV microfocus X-ray source (Nikon Metrology UK, Ltd., Tring, UK) and a Varex 4343N flat panel detector, and later, Nikon's proprietary CLDA (Curved Linear Diode Array) detector.

There are two main challenges to overcome when scanning a dense sample while also requiring the resolution of finer internal details—firstly, to be able to penetrate the pathlengths of the sample [15], and secondly, to overcome the X-ray scattering.

The penetration challenge was overcome by using a high-energy beam, generated by the source, combined with pre-filtering the X-ray beam by using hardware filters to selectively remove the lower energy parts of the generated X-ray spectrum. These are required to be removed since they only contribute to the background of the radiographs and are stopped at the surface of the sample, so do not contribute to the signal within the data. If these were not corrected, the part of the data that is of interest (the anchor) would be compressed due to detector saturation.

The scattering challenge is present due to the interaction of the X-ray beam with the sample itself, where the incident X-ray photon is absorbed, and a new photon is emitted in a different direction [16]. This is an issue within X-ray CT as the generation of the data assumes that the X-rays have travelled in straight lines from the source directly to the given detector pixel. This false illumination (where a photon is scattered onto a pixel, rather than being generated at the source to travel to that pixel) is seen as a blurring within the data, or false brightness in what would otherwise be no material (dark). This presents a specific issue in the internal data since it obscures the details of any features that may be present. The scattering can be reduced by removing the lower energy parts of the spectrum since the lower energy photons are more likely to interact in the overall scattering modes than the higher energy photons (with the range of energies used having a maximum energy of

450 keV) [17]. While this approach can overcome a large amount of the scattering present, it cannot eliminate the scattering sufficiently in more demanding situations.

The second and stronger approach to eliminating the X-ray scattering seen in the data is to reject the scattered X-rays themselves. This can be achieved using Nikon's CLDA, which is a collimated line detector. When this detector is used, the X-ray source is also collimated so that only X-rays that are aligned with the CLDA are released from the source, which turns the beam from a 3D cone (Figure 8) to a near 2D fan (Figure 9).

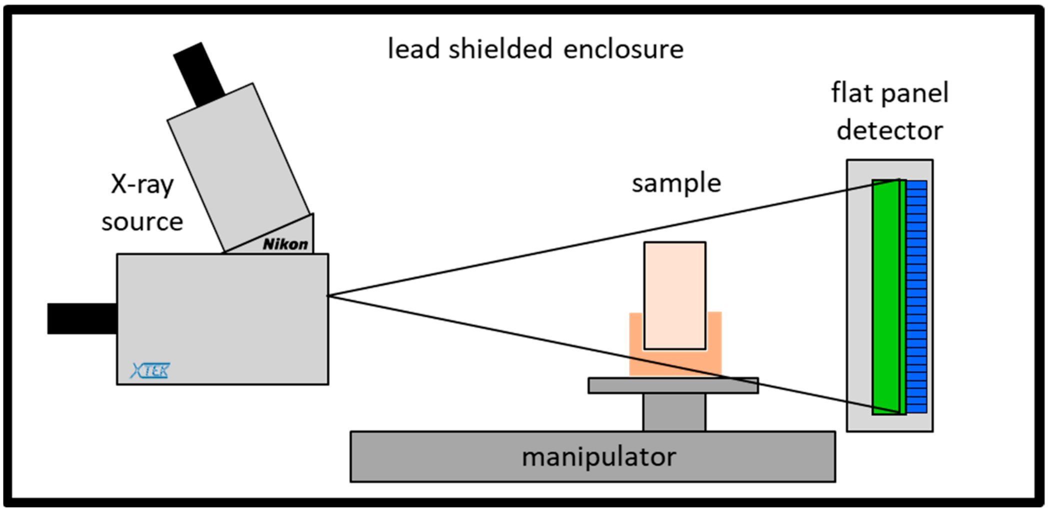


**Figure 8.** The usual set up for a circular CT scan, with an X-ray cone beam targeting the flat panel detector comprising the scintillator (green) and the TFT-diode array (blue).

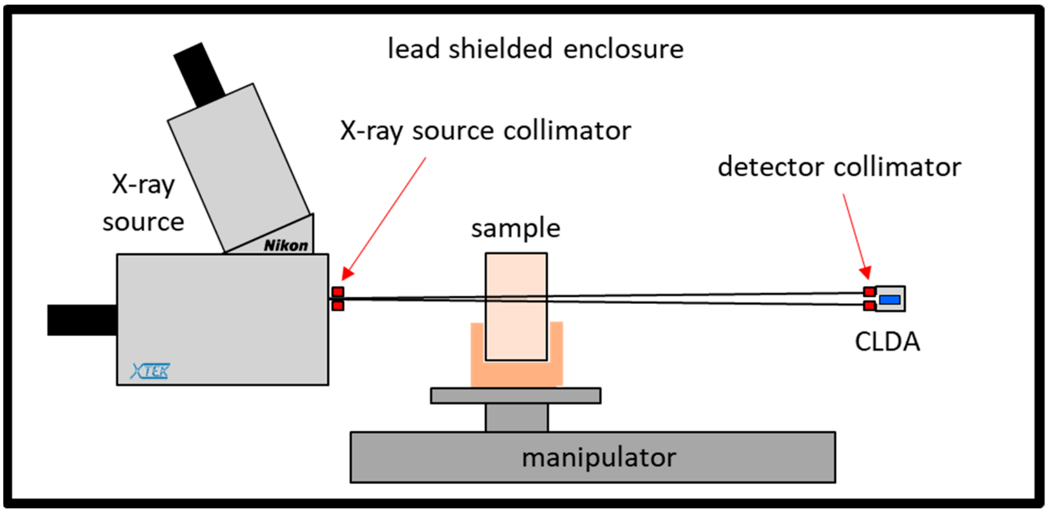


**Figure 9.** The usual set up for a CLDA CT scan. The source has been collimated to produce a fan beam, and the detector is collimated to reject any scattered X-rays.

Using this technique means that any X-ray photon that is scattered out of the source-CLDA plane is rejected by the CLDA's collimator.

Using the CLDA in this case was beneficial over a Linear Diode Array, since the CLDA's diodes match the fan beam angle, meaning a thicker scintillator can be used, resulting in a more sensitive detector to the X-rays present. This is because a linear detector is more affected by scattering within the detector as the X-ray photons are incident to the detector at an angle, rather than perpendicular (as is the case with the CLDA).

Furthermore, the curvature of the CLDA ensures that the distances from the source to each pixel are consistent for the entire width (600 mm) of the detector. This is crucial because the intensity of the beam is inversely proportional to the source-to-pixel distance [see Appendix A]. By keeping the distance consistent, it allows for an even distribution across the detector without having to apply stronger image corrections near the edges of the detector.

An additional feature that aided the stability of the CLDA imaging is that the detector is liquid cooled, meaning that during longer scans, the quality of the data will be more consistent than if the detector were allowed to vary in temperature across the scan duration.

The final settings used for the scanning works are presented in Table 1 below.

**Table 1.** Summary of scanning parameters and results of the study.

| Parameter | 4343N Setup | CLDA Setup |
|---|---|---|
| X-ray source potential | 445 kV | 440 kV |
| X-ray source potential | 215 W | 402 W |
| Effective pixel size | 85.4 µm | 243 µm |
| Beam filtration | 2 mm Pb | 10 mm Cu |
| Scan time | 75 min | 2.3 min per slice |
| Number of slices | n/a | 12 |
| Slice spacing | n/a | 15 mm |
| Results | Indication of internal features | Greater detail of internal features |

## 3. Results

It was decided to initially use the 4343N detector due to the larger volume of the sample being scanned for a given amount of time. The results from the scans using this detector (Figures 10 and 11) showed some details and confirmed that there were internal features to be seen, but subsequently, it was decided to progress to the stronger CLDA approach.

The single-day time constraint was the reason for the limited number of slices, but the slice spacing was set to sample a larger range of the anchor to better indicate the internal features present in the length of the shank.

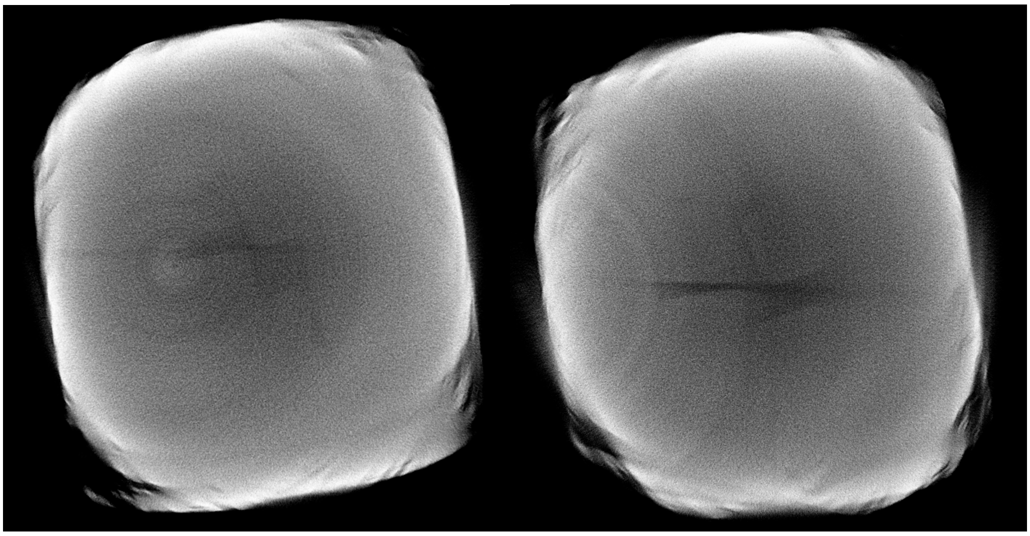

**Figure 10.** Cross-sectional view of the shaft from the circular CT scan. The shank sections are approximately 80 mm wide and 90 mm tall.

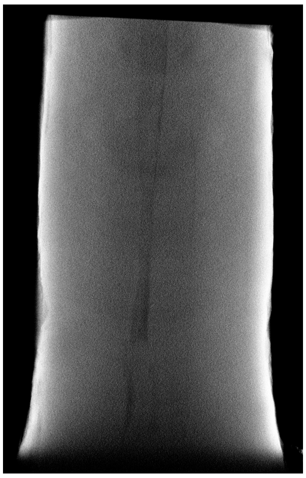

**Figure 11.** Axial slice through the height of the scanned section of shank. A substantial central air channel can be seen. The height of the dataset shown is 170 mm.

The features seen are limited by the X-ray scattering, but there is a distinct low density (most likely air, possibly some slag) region that extends through the entire scanned section. In the images, the data appear to have a higher density at the edges (a brighter white); this, however, is an artefact from the CT scan—beam hardening. While this could be corrected during the data volume generation, it was decided that since correcting this would increase the noise in the dataset, it would be sufficient to take this artefact into account when analysing the dataset manually, with the main interest being the features present near the centre of the shaft.

The results from the CDLA scans (Figure 12) showed greater detail, where internal features could be clearly identified. With the scattering reduced by using the CLDA, the gaps within the shank can now be resolved. The central gap that was seen in the scan using the 4343N detector can be seen much more clearly, with the size and shape changing over the length of the shaft.

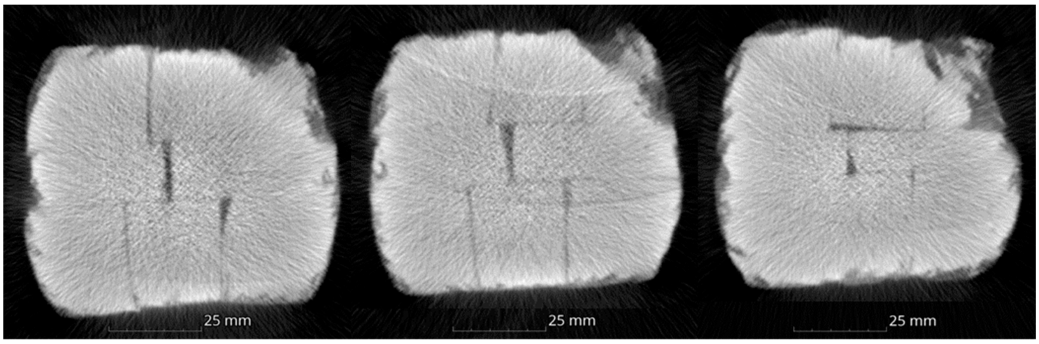


**Figure 12.** Cross-sectional view of the CLDA scan. The shank sections appear to be constructed of individual units that are joined together. Slices are different distances from the datum height (106.3 cm) on the shaft, from left to right: 7.5, 37.5 and 157.5 mm.

The Nikon imaging appears to show eight components to the shank. These units have been interpreted here as six square-section bars and two rectangular-section bars of unknown length. The dimensions are approximately 27 × 27 mm for the square-section bars and 15 × 36 mm for the rectangular ones (Figure 12). The imaging continues for a length of ~260 mm down the shank and appears to show that the bars are continuous over the length analysed. There are some larger gaps between adjacent bars towards the centre of the shank, where there appears to be poor contact. The bars seem to be uniform in dimension and well consolidated, with parallel sides. The top and bottom surfaces of the shank are flat and parallel, whereas the sides are slightly bulging and rounded. Assuming a density for iron of 7.7 g/cm$^3$, and if each of the imaged components runs the length of the anchor shank, then each unit would weigh between 9 kg and 12 kg.

## 4. Discussion

The Nikon scan provides information on both the anchor assembly and the size and shape of the units used in the assembly. These factors can be used to infer the probable date of the anchor since they change over time with developments in ironmaking and iron forging technology.

### *4.1. Chronological Changes in the Size and Shape of Bar Iron in Europe*

The earliest process for iron smelting was a batch process resulting in a spongey 'bloom' of wrought iron. The bloom was forged by hand to expel most of the trapped slag waste and homogenise the metal, with some material lost in this step. The result is a billet, or bar, of metal, smaller than the original bloom [18]. In the Roman period, most blooms were not much more than 8 kg, as any larger becomes difficult to forge by hand with the technology of the time [19]. Blooms that had undergone little forging could potentially be used to create larger objects, for example, a large iron beam from Catterick, UK, Ref. [20] was assembled using scarf welds in a herringbone formation, from 17 blooms, giving an average weight per bloom of around 7 kg. For good quality bar iron, the bloom would be forged further however, and a substantial proportion of the original bloom weight would be lost in that process; for example, the refined billet from the Roman smelting site at Westhawk Farm, UK, weighed 4.5 kg [21]. In summary, depending on the extent of refinement, some Roman blooms might weigh as much as 12 kg, more often around 8 kg, but a refined bar or billet might be less [20,22].

In the second millennium AD, there was a gradual increase in furnace capacity together with the adoption of waterpower, such that by the 14th century, blooms of around 16–20 kg were being produced [23], perhaps increasing to around 90 kg at the beginning of the fifteenth century. Blast furnaces were adopted around 1500 AD in England, slightly earlier in Continental Europe, which made cast iron, and a large increase in iron output was achieved from around the mid-16th century [23]. Cast iron was unsuitable for many applications, but it could be converted into wrought iron using finery hearths. This again resulted in a large ball of spongey wrought iron which was forged down in a coal-fired chafery hearth. Waterpower was also used to drive large hammers, enabling larger blooms to be forged rapidly into bars.

In the post-medieval period, vast quantities of bar iron were traded throughout Europe [24] and this trade led to an increasing focus on widely standardising bar forms. The size of bar varied depending on the origins of the iron and its intended use, but accounts from an 18th-century Bristol merchant specify different types, whether 'squares' (square section), 'broads' (rectangular section) or 'narrow flats', plus other gauges [23,25]. Common sizes were three-quarter inch squares (~19 mm wide) and 2.5 inch broad (~63 mm wide). Iron trade bars have been recovered from wrecks, again often both square and rectangular cross-sections and in uniform sizes. The Gresham Wreck (~1574, English) contained folded iron bars with a rectangular cross-section ~25 × 90 mm and others with a square cross-section of ~40 × 40 mm to 20 × 20 mm, with an unfolded length of 4 m or 6 m approx., and 60 kg in weight [26]. *Rooswijk* (1740, Dutch) contained square-section bars [27], 28 × 28 mm and rectangular section bars 53 × 16 mm. The Aanloop Molengat Dutch vessel from the 17th century contained vast numbers of iron bars, most rectangular 60 × 15–20 mm, but some with square sections 35 × 35 mm, and at least 2.5 to 3.5 m long. Similarly, the wrought iron artillery found on many vessels, particularly of the 15th to 16th centuries, was constructed from iron bars secured by encircling iron bands in a range of gauges. The 15th-century 'Boxted Bombard' was constructed from rectangular bars with a cross-section of approximately 60 × 20 mm [28], and the larger, contemporary 'Mons Meg' from bars with a 60–70 × 25 mm cross-section [29].

### 4.2. Chronological Changes in Size and Construction of Anchors in Europe

The size and form of anchors are partly dictated by their function and by the size of the ship; however, they are also influenced by the availability of iron and manufacturing technology. The weight and size of most early anchors is low, no more than a few hundred kilograms. Although documentary accounts indicate that half tonne anchors were possible by the 13th/15th centuries, these appear to be exceptions for high status vessels. Votruba [30] describes a rapid increase in size during the 16th century, corresponding with the greater availability of iron due to the adoption of blast furnaces and refining forges, and the ability to efficiently work larger masses into bars with powered large hammers [23].

In the first millennium AD, anchors were likely formed by joining partially consolidated blooms or billets of metal with scarf type welds, as in the 7th/8th-century examples from the Tantura F wreck made from multiple 1.5 to 4 kg blooms [31]. From the early second millennium AD, there are examples of anchors made as composites from multiple batons, each weighing around 5–6 kg [30] (and references therein). This includes examples with complex welded structures built up in stages, like the Bremen Kogge anchor forged from long outer plates sandwiching transverse lengths of a different iron alloy.

By the 16th century, there are examples of anchors constructed by forging bars together lengthwise (lone-bar architecture) using scarf welds in the shank, although these were not very robust [30]; this includes the 16th-century example from Labrador Bay, constructed from three bars with a square section of 90 mm and around 2 m long [32]. These objects are assembled in stages with welds made individually.

By the later seventeenth and early eighteenth centuries, however, documents illustrate anchors being made by teams sledge forging together bundles of bars, and with the potential use of water-powered hammers [30,33]. The bars run the length of the intended shank, and the welds between bars are formed simultaneously at the same stage. Some accounts advise on the arrangement of stacked bars to create anchors of appropriate weights.

### 4.3. Summary

The Nikon scan shows that the shank of anchor WTG_D_154 is made up, in cross-section, of eight substantial bars. Their uniform size and dimensions, combining 'squares' and 'flats', suggest that the anchor dates to the post-medieval period, and that it may be European in origin.

The scan also shows gaps of up to 5 mm, where welds have failed to form between bars, running substantial lengths of the anchor shank. These gaps are particularly pronounced in the centre of the shank and suggest that the bars were forged together in a single process, with the internal welds forming (or not) simultaneously. The flat parallel top and bottom surfaces and bulging sides of the cross-section indicate that the entire shank was forged as one component, rather than assembled incrementally, requiring advanced forging capabilities. This technology was well-established by the 17th-century but absent in the 16th century.

Votruba [30] writes that: 'For the subsequent architectural development, we lack a specifically analysed frame finding', meaning an example of an anchor constructed by a process somewhere in between the incremental joining of single bars and the simultaneous forging of bundles of bars. Anchor WTG_D_154 provides a possible example of this intermediary stage, suggesting a possible date of around the later 16th or 17th centuries.

## 5. Conclusions

The Nikon imaging indicates that the anchor is in fact unlikely to be Roman. The information derived from the CT scanning allowed the date of the artefact to be more accurately estimated through analysis of the size of the component parts (in this case uniform bars, likely running the length of the anchor shank) and how they were assembled, in a regular formation consisting of both square and rectangular cross-sections. The size of the blooms (the porous mass of iron and slag produced by early smelting processes) that would be necessary to make these bars is larger than typical for the Roman period. The size, dimensions and uniformity of the bars are, however, consistent with post-medieval Europe when trade in iron bars was thriving. The size and dimensions of the bars match quite closely the dimensions of bars found on wrecks of the post-medieval period and used to make iron artillery. The anchor shank has been assembled in an unusual fashion, simultaneously forging together eight bars arranged carefully such that welds are staggered. This is potentially an early iterant of the bundle-forging method established for anchor making by the beginning of the 18th century. The evidence therefore suggests anchor WTG_D_154 may date from the later 16th to 17th centuries. The relatively small size and weight of the artefact, together with the segmented arms, are also consistent with that period, since anchor size increased rapidly from the 16th century [30]. Comparison with what are thought to be other examples from the era, and evidence in the CT scans of a small step in the surviving arm of WTG_D_154, indicate that flukes may have originally been attached to the ends of the arms, also inferring manufacture after late Roman times (Figure 13).

**Figure 13.** Detail of the upper face of the surviving arm of WTG_D_154 following disconcertion, indicting the likely presence of a fluke joined above the bend of the segmented final section.

These investigations also allowed determination of subsequent proposals for destructive sampling for metal analysis, which may in turn seek to answer questions concerning the construction and provenance of the anchor, as well as to fix the date even more accurately. Furthermore, the initial 2D radiography results provided a better understanding of the object prior to removal of any outer concretion or corrosion that may have been hiding the form of the surface, as well as markings on it and other components that may have been fused to it [34].

## 6. Future Work

Although the anchor is unlikely to be Roman, it is nevertheless the only confirmed example with this type of assembly and arrangement of bars. Possibilities for further investigation include metallography followed by slag inclusion analysis, which may indicate whether the iron derives from coke-smelted or charcoal-smelted iron. If the anchor is indeed 16th century or earlier, it should have been made using wrought iron from a charcoal-fuelled process, either bloomery iron as found with the Gresham Wreck bars [6], for example, or refined from cast iron made in a charcoal-fuelled blast furnace. Slag inclusion analysis methodology is currently more accurate than carbon dating, particularly if the iron's carbon content is low [7].

In future studies of similar objects, the CLDA would be used for all scanning works since the elimination of the scattering within the data has a much greater benefit than the decrease in voxel resolution.

Once the WTG_D_154 anchor has been exhaustively analysed, it will be desalinated to reduce the harmful chlorides in the iron by a combination of electrolysis (depending on the condition of the iron) and washing, using a 2% sodium hydroxide (caustic soda) solution for both. When chloride levels have been reduced to an optimum concentration of less than 50 ppm in the solution, the specimen will be further washed to remove the caustic soda and dried by infrared heaters. Subsequent mechanical cleaning will be followed by treatment with a dilute tannic acid solution to passivate the iron surface and then application of a coating of microcrystalline wax. Finally, the anchor will be placed into airtight packaging, using a silica gel to maintain relative humidity at less than 15%. Following stabilisation, Ipswich Museum will put this important example of the development of anchor technology on permanent display in 2025.

**Author Contributions:** Conceptualization, B.M.; methodology, B.M., J.F. and S.P.; software, J.F.; validation, J.F.; formal analysis, J.F. and S.P.; investigation, B.M., S.P., H.A. and L.N.; resources, ScottishPower Renewables; data curation, Maritime Archaeology Trust; writing—original draft preparation, B.M., J.F. and S.P.; writing—review and editing, B.M., J.F. and S.P.; visualization, B.M. and J.F.; supervision, Brandon Mason (MAT); project administration, B.M.; funding acquisition, B.M. All authors have read and agreed to the published version of the manuscript.

**Funding:** This research was funded by ScottishPower Renewables in fulfilment of the consent compliance conditions set by the Marine Management Organisation and their advisors Historic England.

**Data Availability Statement:** The raw data supporting the conclusions of this article will be made available by the authors on request.

**Acknowledgments:** The authors would like to acknowledge the support of ScottishPower Renewables who funded the recovery of the historic anchor which was the focus of this study, as well as the post-recovery conservation and programme of analysis of the material. The authors also thank Industrial Metrology Business Unit of Nikon Corporation and in particular Michael Hadland for undertaking imaging and further analysis resulting in this open-access paper. We are very grateful to Mary Rose Archaeological Services for undertaking the anchor conservation, to Historic England for the initial X-radiography and to Peter Northover, Stuart Churchley and Zoe Outram (Historic England) and Fabrizio Ciacchella for their advice during the process, and carpenter Matt Hirst at MDH Carpentry for his skills building the anchor imaging support.

**Conflicts of Interest:** Authors Brandon Mason, Heather Anderson and Heather Anderson were employed by the company Maritime Archaeology Trust. Author James Finch was employed by the company Nikon Metrology. The remaining author declares that the research was conducted in the absence of any commercial or financial relationships that could be construed as a potential conflict of interest.

## Appendix A

Regarding the 'inverse square law' mentioned in Section 2; this is a result from the X-ray source generating a 'cone' beam with an assumed isotropic intensity within it, meaning that at the same distance from the focal point, the beam will have the same intensity regardless of the angle from the centre of the beam.

We can illustrate this in 2D as below:

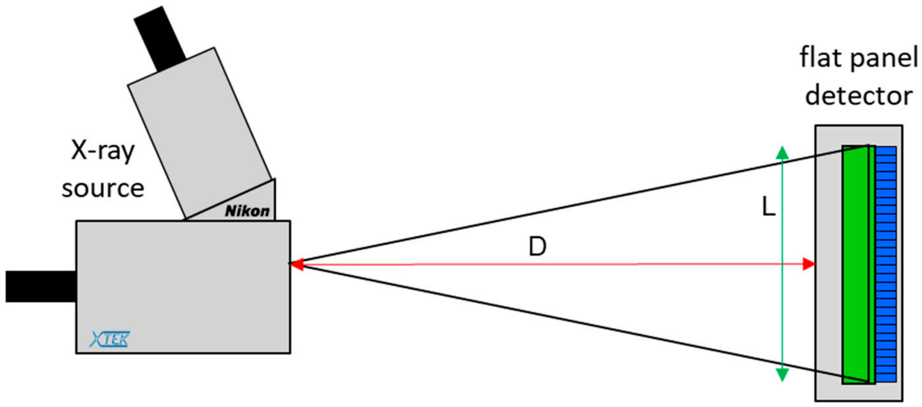


**Figure A1.** Two-dimensional profile of the X-ray and detector setup where D is the source to detector distance, and L is the height of the detector that is illuminated. The flat panel detector comprises the scintillator (green) and the TFT-diode array (blue).

For this discussion, we are assuming that at this distance, the cone beam fully illuminates the detector, with area $A$, where $A = \pi\left(\frac{L}{2}\right)^2$, with an intensity I.

If we now move the detector to twice the distance from the source, we still fully illuminate the panel, but the X-ray cone beam now expands beyond just illuminating the detector panel.

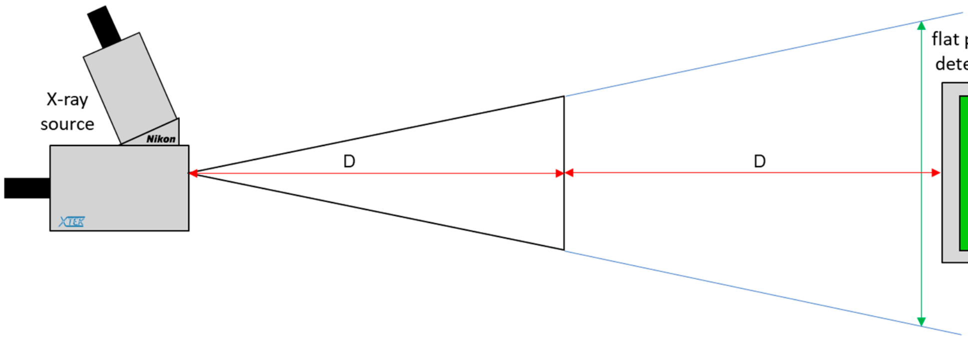


**Figure A2.** The detector has been moved to twice the distance from the X-ray source.

We know that the amount of X-rays present at any cross-sectional slice of the cone beam must be constant since the only source of X-rays is the source itself.

To find the new intensity of the cone beam at this new distance, we need to find the new area. We can achieve this by using a 'similar triangles'-type method since the cone beam angle is consistent between the two positions.

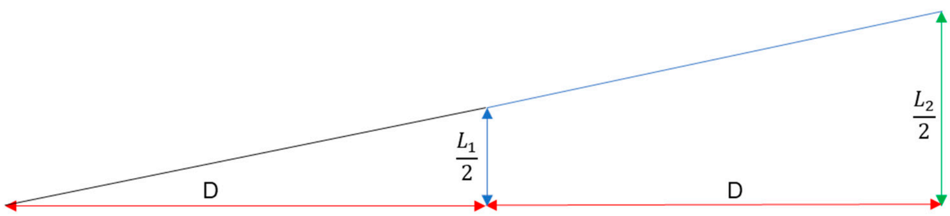


**Figure A3.** The triangles used for calculating the new intensity of the beam.

We can use the $\tan(\theta) = \frac{\text{opposite}}{\text{adjacent}}$, therefore $\tan(\theta) = \frac{\left(\frac{L_1}{2}\right)}{D} = \frac{\left(\frac{L_2}{2}\right)}{2D}$.

Rearranging for $\frac{L_2}{2}$, we achieve: $\frac{L_2}{2} = \frac{2D}{D}\cdot\left(\frac{L_1}{2}\right) = 2\cdot\left(\frac{L_1}{2}\right)$

Now, we can calculate the new area the cone beam illuminates while substituting the knowledge we already have in order to relate it to the original area:

$$A_2 = \pi\left(\frac{L_2}{2}\right)^2 = \pi\cdot\left(2\cdot\left(\frac{L_1}{2}\right)\right)^2 = 4\cdot\pi\left(\frac{L_1}{2}\right)^2 = 4A_1$$

The cone beam now illuminates four times the area it did while at distance D. Since the amount of X-rays across the beam must remain constant, we know that the intensity of the beam must have reduced by a factor of 4.

In summary, the intensity of the beam is inversely proportional to the square of the distance from the source.

## References


1. Cunliffe, B. The Late Iron Age Metalwork from Bulbury, Dorset. *Antiqu. J.* **1972**, *52*, 293–308. [CrossRef]
2. McGrail, S. *Archaeology of Boats in North-West Europe: The Archaeology of Water Transport to AD 1500*; Routledge: Oxford, UK, 1988.
3. Kapitän, G. Ancient Anchors—Technology and classification. *Int. J. Naut. Archaeol.* **1984**, *13*, 33–44. [CrossRef]
4. Tiboni, F. A Roman Iron Anchor from the Port of Genoa, Italy. *Int. J. Naut. Archaeol.* **2014**, *45*, 204–205. [CrossRef]
5. Mason, B. EA ONE Watching Brief on Relocation of Discrete Features; Unpublished archaeological report, 2020a. Maritime Archaeology Ltd./ScottishPower Renewables, EA1-CON-B-IBR-048292 Rev 01.
6. Birch, T.; Martinón-Torres, M. The iron bars from the 'Gresham Ship': Employing multivariate statistics to further slag inclusion analysis of ferrous objects. *Hist. Metall.* **2015**, *48*, 69–78.
7. Clagget, D.; McCarthy, J.; Murray, W.; Seboa, E.; Jouttijärvic, A.; Hülsd, M.; Benjamin, J. Modern or medieval? Analysis of an iron anchor from Camuscross, Scotland and direct dating methods for metal artefacts. *J. Archaeol. Sci. Rep.* **2019**, *25*, 144–152. [CrossRef]
8. Available online: https://www.nauticalarchaeologysociety.org/ct-scan-for-free (accessed on 7 May 2024).
9. Ingvardson, G.T.; Müter, D.; Foley, B.P. Purse of medieval silver coins from royal shipwreck revealed by X-ray microscale Computed Tomography (µCT) scanning. *J. Archaeol. Sci. Rep.* **2022**, *43*, 103468. [CrossRef]
10. Clagget, D. A Typological Assessment of Anchors Used in Northern Europe During the Early and High Middle Ages, CE 750–1300. Master's Thesis, Flinders University of South Australia, Adelaide, Australia, 2017.
11. Jobling, H.J.W. The History and Development of English Anchors ca. 1550 to 1850. Master's Thesis, Texas A&M, College Station, TX, USA, 1993.
12. Mason, B. 2020b EA ONE Post-Recovery Management of Historic Anchor WTG_D_154, Conservation Method Statement; Unpublished archaeological report, 2020b. Maritime Archaeology Ltd./ScottishPower Renewables, EA1-CON-B-IBR-048302.
13. Graham, K. *X-Radiography Report: X-ray of Anchor for Maritime Archaeology Trust*; Unpublished archaeological report, 2021; Historic England: Portsmouth, UK, 2021.
14. Muckelroy, K. *Maritime Archaeology*; Cambridge University Press: Cambridge, UK, 1978.
15. Hubbell, J.H.; Seltzer, S.M. *X-ray Mass Attenuation Coefficients, NIST Standard Reference Database 126—Tables of X-ray Mass Attenuation Coefficients and Mass Energy-Absorption Coefficients from 1 keV to 20 MeV for Elements Z = 1 to 92 and 48 Additional Substances of Dosimetric Interest*; National Inst. of Standards and Technology-PL: Gaithersburg, MD, USA, 1995. [CrossRef]
16. Levine, Z.H.; Blattner, T.J.; Peskin, A.P.; Pintar, A.L. Scatter Corrections in X-Ray Computed Tomography: A Physics-Based Analysis. *J. Res. Natl. Inst. Stand. Technol.* **2019**, *124*, 124013. [CrossRef] [PubMed]
17. Biggs, F.; Lighthill, R. *Analytical Approximations for X-ray cross Sections III*; Sandia National Lab (SNL-NM): Albuquerque, NM, USA, 1988. [CrossRef]
18. Historic England. *Archaeometallurgy: Guidelines for Best Practice*; Historic England: Swindon, UK, 2015.
19. Sauder, L. An American bloomery in Sussex. In *Accidental and Experimental Archaeometallurgy*; Dungworth, D., Doonan, R.C.P., Eds.; Historical Metallurgy Society: London, UK, 2013; pp. 69–74.
20. Starley, D. Metallurgical study of an iron beam from Catterick bypass (site 433). In *Roman Catterick and Its Hinterland. Excavations and Research, 1958–1997*; Wilson, P.R., Ed.; Part II, CBA Research Report 129; CBA: Swindon, UK, 2002; pp. 166–172.
21. Paynter, S. Romano-British workshops for iron smelting and smithing at Westhawk Farm, Kent. *J. Hist. Metall. Soc.* **2007**, *41*, 15–31.
22. Tylecote, R.F. *The Prehistory of Metallurgy in the British Isles*; Routledge: London, UK, 1990.
23. Schubert, H.R. *History of the British Iron and Steel Industry from c. 450 B.C. to A.D. 1775*; Routledge: London, UK, 1957.
24. King, P. The production and consumption of bar iron in early modern England and Wales. *Econ. Hist. Rev.* **2005**, *57*, 1–33. [CrossRef]
25. Evans, C.; Rydén, G. *Baltic Iron in the Atlantic World in the Eighteenth Century*; Brill: Boston, MA, USA, 2007.
26. Auer, J.; Firth, A. The 'Gresham Ship'. *Post-Mediev. Archaeol.* **2007**, *41*, 222–241. [CrossRef]
27. Wessex Archaeology. *Rooswijk, Goodwin Sands—Designated Site Assessment: Archaeological Report*; Ref: 53111.03ddd; Wessex Archaeology: Salisbury, UK, 2007.

28. Blackmore, H.L. The Boxstead Bombard. *Antiqu. J.* **1987**, *67*, 86–96. [CrossRef]
29. Smith, R.D.; Brown, R.R. *Bombards: Mons Meg and Her Sisters (Royal Armouries Monograph 1)*; Trustees of the Royal Armouries: London, UK, 1989.
30. Votruba, G. Technology of Iron Anchor-Frame Production in the Age of Exploration. In *Heritage and the Sea, Volume 2: Maritime History and Archaeology of the Global Iberian World (15th–18th Centuries)*; Crespo Solana, A., Ed.; Springer: New York, NY, USA, 2022; Volume 2, Chapter 12; pp. 273–296. [CrossRef]
31. Aronson, A.; Ashkenazi, D.; Barkai, O.; Kahanov, Y. Archaeometallurgical investigation of the iron anchor from the Tantura F shipwreck. *Mater. Charact.* **2013**, *78*, 108–120. [CrossRef]
32. Light, J.D. The 16th century anchor from Red Bay, Labrador. *Int. J. Naut. Archaeol. Underw. Explor.* **1990**, *19*, 307–316. [CrossRef]
33. Gay, J. *Six Millénaires d'Histoire des Ancres*; Histoire maritime: Paris, France, 1997.
34. Historic England. *Guidelines on the X-Radiography of Archaeological Metalwork, 9234*; Historic England: Swindon, UK, 2006.